



Gazi University

Journal of Science

PART A: ENGINEERING AND INNOVATION

<http://dergipark.org.tr/gujisa>

Effectuality of the Frequency Levels on the C&G/ ω -V Data of the Polymer Interlayered Metal-Semiconductor Structure

Jaafar Abdulkareem Mustafa ALSMAEL¹  Nuray URGUN²  Serhat Orkun TAN^{3*}  Habibe Uslu TECİMER⁴ ¹Karabük University, Department of Electrical and Electronics Engineering, 78050, Karabük, Türkiye²Karabük University, Faculty of Technology, Department of Mechatronics Engineering, 78050, Karabük, Türkiye³Karabük University, Faculty of Technology, Department of Electrical Engineering, 78050, Karabük, Türkiye⁴Karabük University, Faculty of Engineering, Department of Medical Engineering, 78050, Karabük, Türkiye

Keywords	Abstract
Metal-Polymer-Semiconductor Structures	Voltage and frequency dependent of capacitance and conductivity versus voltage (C&G/ ω -V) qualifications of Al/(ZnFe ₂ O ₄ -PVA)/p-Si structure was compared and examined at lower and higher frequencies as 10 kHz and 1 MHz, respectively. The negative capacitance (NC) is a phenomenon that occurs at low frequencies and is primarily caused by minority carrier injection, series resistance (R_s), and surface states (N_{ss}). Because of the specific density distribution and relaxation times of N_{ss} , NC acts different behavior at lower and higher frequency levels and loses its effectiveness with increasing frequency. Also, the fluctuations in C and G/ ω were ascribed to doping concentration, surface states loss charges, and interlayer thickness. N_{ss} was acquired using the low-high frequency capacitance method (C_{LF} - C_{HF}), and the forward biased C^{-2} vs V graphs (at 10 kHz to 1 MHz) were used to determine the Fermi level (E_F), barrier height (Φ_B), and concentration of doped acceptor atoms (N_A). Accordingly, it has been detected that C and G/ ω are highly dependence on biases and frequencies. Then again, the polarizations and surface states effect are barely perceptible at extremely higher frequency levels. Thus, polarization and R_s stand out as important parameters that should be taken into account when examining the basic parameters of electronic devices.
Surface States	
Negative Capacitance	
Series Resistance	
Frequency	

Cite

Alsmael, J. A. M., Urgun, N., Tan, S. O., & Uslu Tecimer, H. (2022). Effectuality of the Frequency Levels on the C&G/ ω -V Data of the Polymer Interlayered Metal-Semiconductor Structure. GU J Sci, Part A, 9(4), 554-561.

Author ID (ORCID Number)	Article Process	
J. A. M. Alsmael, 0000-0002-2426-9421	Submission Date	17.11.2022
N. Urgun, 0000-0001-6574-4287	Revision Date	16.12.2022
S. O. Tan, 0000-0001-6184-5099	Accepted Date	21.12.2022
H. Uslu Tecimer, 0000-0002-0094-7427	Published Date	31.12.2022

1. INTRODUCTION

Metal and semiconductors are often used together in electronic technology, and metal-semiconductor (MS) structures or Schottky junctions are used in electronic/semiconductor devices, especially as switching elements (Sze, 1981; Bakkaloğlu et al., 2021). MS structures are used in different ways, and MIS, MPS and MFS structures are obtained by using insulator, polymer, and ferroelectric interlayers, respectively. Thereby, an organic/polymer interlayer between the metal and semiconductor forms the MPS structure. A semi-crystalline polymer that is water soluble is called polyvinyl alcohol (PVA), which has a hydroxyl group (OH-) and many hydrogen bonds in its structure. An all-purpose material, PVA, can be utilized in distinct kind of applications such as cements, mortars, films, fibers, and polymerization stabilizers. Since it has a very stable chemical and physical structure, many researchers have confirmed its qualities, and it has a variety of applications in nanotechnology (Gaaz et al., 2015; Aziz, 2016). Furthermore, organic/polymer doped nanocomposite material can be easily coated on a semiconductor layer at average temperature by using electrospinning technique which is provided by a collector and a high voltage power supply also with some equipment of nozzle and syringe pump (Unnithan et al., 2015). At the same time, PVA, which has a high dielectric strength but low electrical conductivity, increases its electrical and optical features when it is doped with a dopant material with high

*Corresponding Author, e-mail: serhatorkuntan@karabuk.edu.tr

conductivity (Subba Reddy et al., 2006). Zinc ferrite (ZnFe_2O_4) was chosen as a dopant material in this study due to its properties that can contribute to the charge transitions between metal and semiconductor.

Zinc ferrite is not only of interest for essential examination in magnetization, but ferrites also have low-hole semiconductors and separators at low temperatures; they have been utilized in various technologically significant applications, for example, gas sensors (Patil et al., 2014), magnetization materials (Vijatović-Petrović et al., 2020), photocatalysis (Hou et al., 2018), catalysts (Zhang et al., 2015), and absorbance materials (Shultz et al., 2006). Moreover, for medical and industrial purposes, zinc ferrite has been developing immensely since the most recent decade. Zinc ferrite nanoparticles have additionally been utilized for media capacity, ferrofluids, spintronic, magnetic refrigeration, drug conveyance to specific areas of the body, hyperthermia, and biosensors, etc. (Slavu et al., 2021).

The structure's series resistance, the interface states between the metal and the semiconductor, and the barrier height are considered among the performance factors of the polymer interlayered junction. The resistance and doped-polymer interlayer are essential components of the MPS structure. Because both the series resistance and the depletion layer share the total voltage applied to the structures (Tecimer et al., 2018). As a result, the quality of the interlayer and the series resistance were an essential impact on the dependability and usefulness of these devices (Zeyrek et al., 2013).

In this study, considering its possible future mass production, it is aimed to fabricate a low-cost electronic circuit element with easy production techniques, instead of conventional (MS) structures with insulator (interface oxide) interlayer, which is widely researched in the literature. For this purpose, the operation of this circuit element at low and high frequencies was examined in the light of parameters such as series resistance and interface conditions, and the most appropriate frequency-operation range was tried to be determined. Thanks to this research, it has been interpreted that, how the electrical parameters of the fabricated semiconductor-based circuit element varied by frequency. Inferences were made about how the positive and negative effects of the relevant parameters affect the performance of the structure at the related frequencies. The comparison of low and high frequencies in this study is important to better understand the operation of Schottky structures operating at high frequencies and known for their rapid response to forward and reverse biases.

2. MATERIALS AND METHODS/EXPERIMENTAL METHODS

In order to prepare the $\text{Al}/(\text{ZnFe}_2\text{O}_4\text{-PVA})/\text{p-Si}$ structure, the Zinc ferrite nanoparticles doped PVA solution is precipitated on the wafer employing the electro-spinning process. In the earlier study (Alsmael et al., 2022) specifications of the deposition and manufacturing process are provided. Impedance Analyzer (4192A LF) (5 Hz–13 MHz) was employed to acquire C-V and G/ ω -V data. In addition, Janis vpf-475, which was designed to minimize the influence of external factors on the measured values, was used throughout the experimental process. Figure 1 depicts the schematic diagram of the measurement setup as below.



Figure 1. The schematic presentation of the experimental setup (Alsmael et al., 2022)

3. RESULTS AND DISCUSSIONS

As generally known, MS-type and MIS or MPS-type contacts indicate different properties from each other. This difference is a result of the interlayer formation with a wide variety of production techniques, which helps regulate charge transitions and provide more stable conduction/isolation states. The presence of an interlayer between the metal and the semiconductor significantly changes the structure's C-V and G/ω -V properties compared to the ideal or Schottky barrier diodes MS type. Figure 2 and 3 presents the (C and G/ω) versus voltage data for Al/(ZnFe₂O₄ -PVA)/p-Si type at ordinary room temperatures, respectively. Three distinct regions are clearly seen in Figure 2, as a region of reflection (4 V to 0V), depletion (0 V to -1V), and accumulation (-1 V to -4 V) for low frequencies in the ± 4 V voltage range. C values increase with decreasing voltage. The capacitance values display three peaks starting in the forward bias region with negative capacitance and continuing with two peaks in the reverse bias. Peaks in capacitance signal the presence of interface states. The cause for this characteristic behavior can be referred to the ZnFe₂O₄ -PVA interface and the presence of series resistors. G/ω values peak at the depletion zone and reduce with increasing frequency due to the density distribution at the device interface (Çetinkaya et al., 2019).

As demonstrated in Figure 2 and 3 the C and G/ω values were nearly constant at 1 MHz high frequency compared to 10KHz low frequency because interface charges cannot be tracking the AC signal at high frequencies and do not make a contribution to the observed capacitance values (Neamen, 1992).

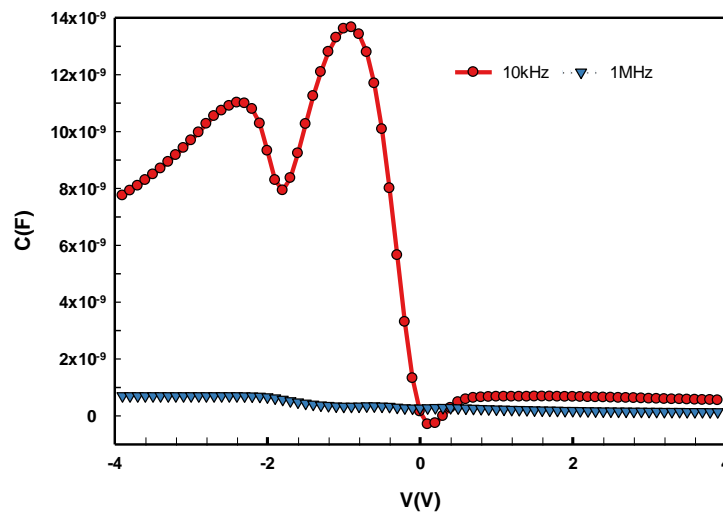


Figure 2. C-V curves for the low and high frequencies

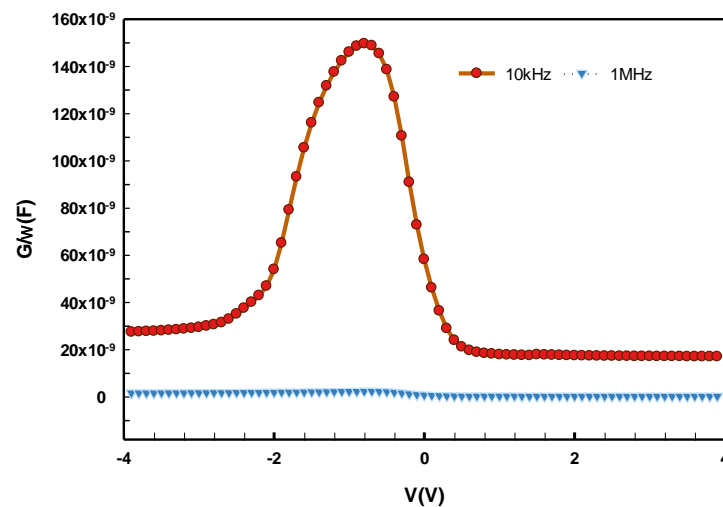


Figure 3. G/ω -V curves for the low and high frequencies

Using the conductance approach, it was capable to determine the R_s of the contacts by the admittance measuring, where C_m and G_m stand for the experimentally measured capacitance and conductance, respectively.

$$R_s = \frac{G_m/\omega}{\omega[(G_m/\omega)^2 + C_m^2]} \quad (1)$$

As shown in the equation, the series resistance is reversely proportional with the sum of the square of the C_m and G_m/ω multiplied by the angular frequency(ω). On the other hand, it is directly proportional to the conductance, so the series resistance decreases through the increased capacitance with the conductivity. As observed, the values of capacitance and conductivity in the forward biases are lower than in the reverse biases.

Among the reasons for the series resistance formation, the semiconductor's bulk resistance, the contact resistance between the semiconductor and the metal, the rectifier and ohmic contact resistances and possible resistances of the metal electrodes are effective.

Figure 4 represents the R_s -V curves for lower (10 kHz) and higher (1 MHz) frequency with reverse and forward bias voltages variations. While the R_s value stayed steady in the reverse bias region at 1 MHz frequency, the R_s value at 10kHz increases with increasing forward and reverse biases.

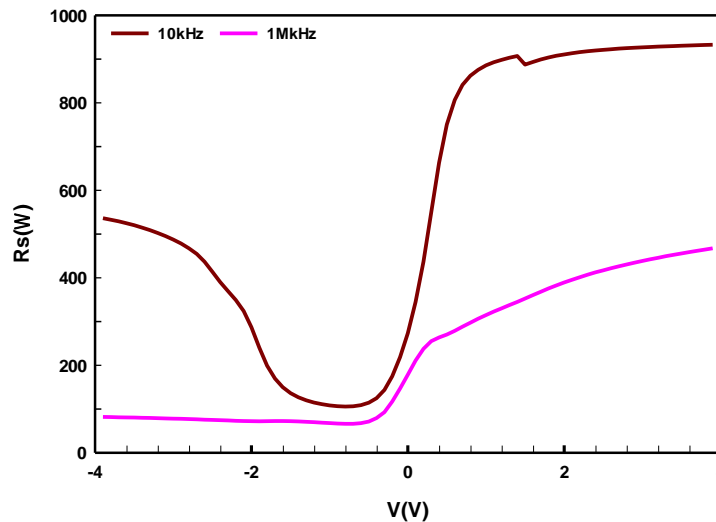


Figure 4. R_s -V curves for the low and high frequencies

The (C_{LF} - C_{HF}) method is useful for obtaining the voltage-dependent distribution of the interface state density, N_{ss} (V). This method allows easy calculation of many features of the interface layer and semiconductor interface (Ata et al., 2022). The following equation can be used to get N_{ss} (V) values of ZnFe₂O₄ -PVA interlayered Al/p-Si structure. N_{ss} (V)-V graphs for the structure was formed utilizing high-frequency (1 MHz) and low-frequency (10 kHz) values.

$$N_{ss} = \left(\frac{1}{qA}\right) \left[\left(\frac{1}{C_{LF}} - \frac{1}{C_{ox}}\right)^{-1} - \left(\frac{1}{C_{HF}} - \frac{1}{C_{ox}}\right)^{-1} \right] \quad (2)$$

The explanations of each abbreviation are given as; A; the area of the MPS structure, q; the electronic charge, C_{ox} ; the capacitance of the insulating layer, and d; the thickness of the polymer film. 10 kHz and 1 MHz were performed in this situation as the low and high frequencies. Figure 5 illustrates the N_{ss} -V curve, which has two peaks at around 1 V and 2.4 V at reverse biases. The disruption of the periodic lattice structure on the crystal surface and the density distribution in the finite band gap of the semiconductor may be related to the causes of these peak formations (Ata et al., 2022). The density of the interface states in the C and G_m/ω graphs acquired at high frequency (1MHz) may be ignored since interface states can only track AC signals at frequencies below 500 kHz (Neamen, 1992).

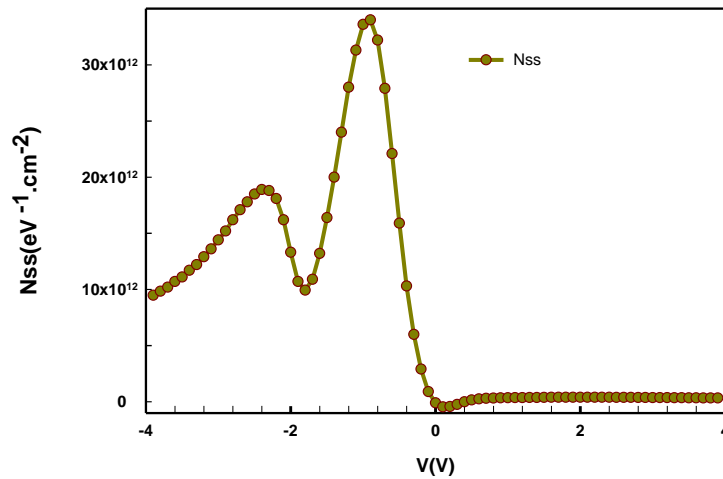


Figure 5. N_{ss} -V curve of the MPS structure

The graph for $1/C^2$ of the related structure was drawn for the low and high frequencies, 10 kHz and 1 MHz level, and presented below in Figure 6.

$$C^{-2} = \frac{2(V_0 + V_F)}{q\epsilon_s\epsilon_0A^2N_A} \tag{3}$$

Here, V_F is the forward bias voltage, ϵ_s is the relative permittivity of the semiconductor, ϵ_0 is the permittivity of free space or vacuum, and V_0 is the cut-off voltage at zero volts. It is evident that these curves behave linearly well in the forward bias range of 1.5 to 3 V.

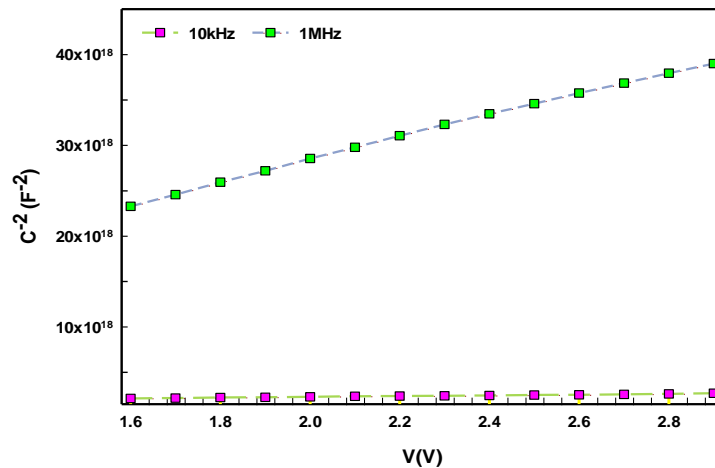


Figure 6. $1/C^2$ -V curves for the low and high frequencies

Based on the voltage evolution of $1/C^2$ for the device presented in Figure 7 and 8, the Fermi-energy level E_F (eV) $\ln(f)$, barrier height (Φ_B) $\ln(f)$, and concentration of doped acceptor atoms (N_A) $\ln(f)$ were determined by using following equation:

$$E_F = \frac{kT}{q} \ln\left(\frac{N_V}{N_A}\right) \tag{4}$$

Here, the density of active states in Si valence band is symbolized with N_V . The following equation were used to get Φ_B (C-V) values:

$$\Phi_B(C - V) = \left(V_0 + \frac{kT}{q}\right) + E_F \tag{5}$$

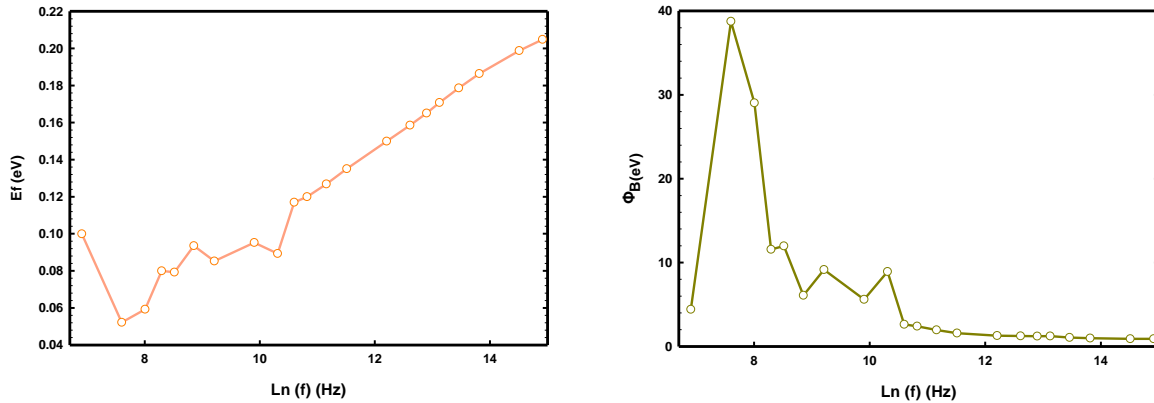


Figure 7. Ln frequency dependent a) E_f (eV) and b) Φ_B curves of the device

Concentration of doped acceptor atoms (N_A) values were obtained using the following equation.

$$N_A = \frac{2}{q\epsilon_S\epsilon_0 A^2 \tan(\theta)} \tag{6}$$

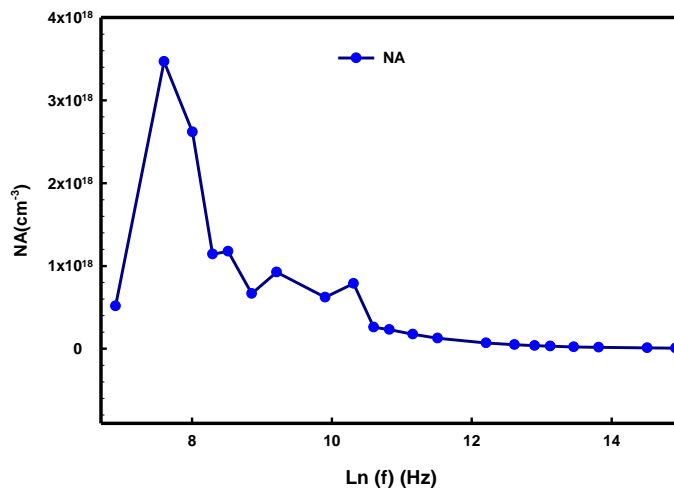


Figure 8. Ln frequency dependent N_A (cm^{-3}) curve of the device

4. CONCLUSION

Electrical measurements of the PVA interlayered MS device were made by utilizing C&G/ ω -V data at frequency and voltage ranges of 10 kHz–1 MHz and -4V– +4V, respectively. The capacitance, conductance, series resistance, and the voltage evolution of $1/C^2$ were compared between low frequency (10KHz) and high frequency (1 MHz) as a function of biasing voltage. From the plot of C-V, the structure showed a negative capacitance characteristic behavior. Estimation of electrical parameters of the structure such as Fermi-energy level E_f (eV) $\ln(f)$, barrier height (Φ_B) $\ln(f)$ and concentration of doped acceptor atoms (N_A)(cm^{-3}) $\ln(f)$ was performed by utilizing the $1/C^2$ voltage evolution. In order to better interpret the performance of the structure on the basis of frequencies, it would be more accurate to interpret the experimental results by considering the behavior in the reverse and forward polarization regions. Especially for the reverse polarity, higher capacitance and conductance values are seen for low frequency, while the capacitance and conductance values at forward polarization region are almost close to each other for both frequencies. Looking at the series resistance values; higher series resistance values were obtained at low frequency in both reverse and forward polarizations. In addition to these, the fact that the interface states are higher in the reverse polarity region can be interpreted as the performance of the structure in this region, especially for low frequency, is more inadequate. The effects of the increase in frequency are observed as a decrease on the capacitance, conductance, and series resistance values, especially in the reverse bias region. Experimental results point out that, the electrical qualifications of

the device are very sensitive to the applied biases and especially to the frequency levels. Considering signal tracking difficulty at high frequencies, such effects of series resistance, interface states, negative capacitance have been decreased for the fabricated device. In terms of devices operating at high frequencies, the effects of the parameters obtained for this fabricated contact structure at low frequency and in the reverse polarization region may have a negative effect in terms of rapid response to polarization variations. On the other hand, the decrease in the effect of these parameters at high frequency is evaluated positively in terms of fast switching performance.

ACKNOWLEDGEMENT

Some part of this study is presented at 9th International Conference on Materials Science and Nanotechnology for Next Generation (MSNG-2022).

REFERENCES

- Alsmael, J. A. M., Tan, S. O., Tecimer, H. U., Altındal, Ş., & Kalandaragh, Y. A. (2022). The Impact of Dopant on the Dielectric Properties of Metal-Semiconductor With ZnFe₂O₄ Doped Organic Polymer Nanocomposites Interlayer. *IEEE Transactions on Nanotechnology*, 21, 528-533. doi:[10.1109/TNANO.2022.3207900](https://doi.org/10.1109/TNANO.2022.3207900)
- Ata, D., Altındal Yeriskin, S., Tataroğlu, A., & Balbasi, M. (2022). Analysis of admittance measurements of Al/Gr-PVA/p-Si (MPS) structure. *Journal of Physics and Chemistry of Solids*, 169, 110861. doi:[10.1016/j.jpics.2022.110861](https://doi.org/10.1016/j.jpics.2022.110861)
- Aziz, S. B. (2016). Modifying Poly(Vinyl Alcohol) (PVA) from Insulator to Small-Bandgap Polymer: A Novel Approach for Organic Solar Cells and Optoelectronic Devices. *Journal of Electronic Materials*, 45(1), 736-745. doi:[10.1007/s11664-015-4191-9](https://doi.org/10.1007/s11664-015-4191-9)
- Bakkaloğlu, Ö. F., Ejderha, K., Efeoğlu, H., Karataş, Ş., & Türüt, A. (2021). Temperature dependence of electrical parameters of the Cu/n-Si metal semiconductor Schottky structures. *Journal of Molecular Structure*, 1224, 129057. doi:[10.1016/j.molstruc.2020.129057](https://doi.org/10.1016/j.molstruc.2020.129057)
- Çetinkaya, H. G., Sevgili, Ö., & Altındal, Ş. (2019). The fabrication of Al/p-Si (MS) type photodiode with (%2 ZnO-doped CuO) interfacial layer by sol gel method and their electrical characteristics. *Physica B: Condensed Matter*, 560, 91-96. doi:[10.1016/j.physb.2019.02.038](https://doi.org/10.1016/j.physb.2019.02.038)
- Gaaz, T. S., Sulong, A. B., Akhtar, M. N., Kadhum, A. A. H., Mohamad, A. B., Al-Amiery, A. A., & McPhee, D. J. (2015). Properties and applications of polyvinyl alcohol, halloysite nanotubes and their nanocomposites. *Molecules*, 20(12), 22833-22847. doi:[10.3390/molecules201219884](https://doi.org/10.3390/molecules201219884)
- Hou, G., Li, Y., & Wang, X. (2018). Research Progress of Zinc Ferrite as Photocatalyst. *Cailiao Daobao/Materials Review*, 32(1), 51-57. doi:[10.11896/j.issn.1005-023X.2018.01.006](https://doi.org/10.11896/j.issn.1005-023X.2018.01.006)
- Neamen, D. A. (1992). *Semiconductor Physics and Devices, Basic Principles*. McGraw-Hill.
- Patil, J. Y., Nadargi, D. Y., Gurav, J. L., Mulla, I. S., & Suryavanshi, S. S. (2014). Glycine combusted ZnFe₂O₄ gas sensor: Evaluation of structural, morphological and gas response properties. *Ceramics International*, 40(7) Part B, 10607-10613. doi:[10.1016/j.ceramint.2014.03.041](https://doi.org/10.1016/j.ceramint.2014.03.041)
- Shultz, M. D., Carpenter, E. E., Morrison, S. A., & Calvin, S. (2006). Cation occupancy determination in manganese zinc ferrites using Fourier transform infrared spectroscopy. *Journal of Applied Physics*, 99(8), 08M901. doi:[10.1063/1.2151831](https://doi.org/10.1063/1.2151831)
- Slavu, L. M., Rinaldi, R., & Di Corato, R. (2021). Application in nanomedicine of manganese-Zinc ferrite nanoparticles. *Applied Sciences*, 11(23), 11183. doi:[10.3390/app112311183](https://doi.org/10.3390/app112311183)
- Subba Reddy, C. V., Han, X., Zhu, Q.-Y., Mai, L.-Q., & Chen, W. (2006). Dielectric spectroscopy studies on (PVP + PVA) polyblend film. *Microelectronic Engineering*, 83(2), 281-285. doi:[10.1016/j.mee.2005.08.010](https://doi.org/10.1016/j.mee.2005.08.010)
- Sze, S. M. (1981). *Physics of Semiconductor Devices*. (2nd edition). Wiley-Blackwell.
- Tecimer, H. U., Alper, M. A., Tecimer, H., Tan, S. O., & Altındal, Ş., (2018). Integration of Zn-doped organic polymer nanocomposites between metal semiconductor structure to reveal the electrical qualifications of the diodes. *Polymer Bulletin*, 75(9), 4257-4271. doi:[10.1007/s00289-018-2274-5](https://doi.org/10.1007/s00289-018-2274-5)

- Unnithan, A. R., Arathyram, R. S., & Kim, C. S. (2015). Chapter 3 - Electrospinning of Polymers for Tissue Engineering. In: S. Thomas, Y. Grohens, & N. Ninan (Eds.), *Nanotechnology Applications for Tissue Engineering* (pp. 45-55). William Andrew Publishing. doi:[10.1016/B978-0-323-32889-0.00003-0](https://doi.org/10.1016/B978-0-323-32889-0.00003-0)
- Vijatović-Petrović, M. M., Džunuzović, A., Bobić, J. D., Ilić, N., Stijepović, I., & Stojanović, B. D. (2020). Study of barium titanate/nickel-zinc ferrite based composites: Electrical and magnetic properties and humidity sensitivity. *Processing and Application of Ceramics*, 14(1), 9-18. doi:[10.2298/PAC2001009V](https://doi.org/10.2298/PAC2001009V)
- Zeyrek, S., Acaroğlu, E., Altındal, Ş., Birdoğan, S., & Bülbül, M. M. (2013). The effect of series resistance and interface states on the frequency dependent C-V and G/w-V characteristics of Al/perylene/p-Si MPS type Schottky barrier diodes. *Current Applied Physics*, 13(7), 1225-1230. doi:[10.1016/j.cap.2013.03.014](https://doi.org/10.1016/j.cap.2013.03.014)
- Zhang, F., Wei, C., Hu, Y., & Wu, H. (2015). Zinc ferrite catalysts for ozonation of aqueous organic contaminants: Phenol and bio-treated coking wastewater. *Separation and Purification Technology*, 156, Part 2, 625-635. doi:[10.1016/j.seppur.2015.10.058](https://doi.org/10.1016/j.seppur.2015.10.058)